Turbulence and Structure Formation Associated with Vortex Dynamics in Non-Neutral Plasma Flow

Yasuhito KIWAMOTO[1,2], Yosuke KAWAI[1], Yukihiro SOGA[1,3] and Jun AOKI[1,4]

[1]*Graduate School of Human and Environmental Studies, Kyoto University, Sakyo-ku, Kyoto 606-850, Japan*
[2]*Professor Emeritus, Kyoto University*
[3]*School of Mathematics and Physics, Kanazawa University, Kanazawa-shi 920-1192, Japan*
[4]*Graduate Shcool of Science, Osaka University, Toyonaka-shi 560-0043, Japan*

(Received 6 December 2009 / Accepted 22 January 2010)

We discuss generation processes of two distinct structures, ordered arrays of high density clumps and single-peaked macroscopic structures as observed in relaxation processes starting from non-equilibrium distributions of strongly magnetized pure electron plasmas. The two-dimensional character of the guiding-center system shows equivalence between the distributions of electron density and the vorticity in $E\times B$ flow. Observations reveal decisive role of fluctuations in the ambient electrons in assisting the formation of ordered arrays and their destruction that successively leads to next stage of ordered structures. The fluctuating parts extracted via wavelet analyses show characteristic features of spectrum and k-space dynamics in ideal 2D turbulence. Such dynamics interpreted as ideal 2D fluid actually reflect electromagnetic dynamism of charged particle subject to redistribution of potential energy and angular momentum. One extra feature of 2D vortex dynamics of electrons is the contribution of Landau-damping of collective particles' motion which conveys externally applied electromagnetic field to the bulk electrons via resonant electrons as a source of energy and momentum.

Keywords: non-neutral plasma, vortex dynamics, vortex crystal, structure formation, turbulence, enstrophy cascade, wavelet analysis, Landau-damping

DOI: 10.1585/pfr.5.S2002

1. Introduction

The macroscopic dynamics of the guiding-center particles of non-neutral plasmas (NNP's) in the plane transverse to homogeneous magnetic field B are isomorphic to those of the two-dimensional (2D) Euler fluids. Within this approximation, in pure electron plasmas, the distributions of electron density $n(x,y)$ and the electrostatic potential $\phi(x,y)$ are related to the vorticity $\zeta(x,y)$ and stream function $\psi(x,y)$ as $\vec{\zeta}(x,y) = \nabla\times(\vec{E}\times\vec{B}/B^2) = \hat{z}\triangle\phi/B = en(x,y)\hat{z}/\varepsilon_0 B$ and $\psi(x,y) = \phi(x,y)/B$, where ε_0 is the dielectric constant in vacuum [1].

Due to the absence of counter-charged particles, the canonical angular momentum of the NNP system is enhanced over kinetic component by several orders of magnitudes owing to the contribution of azimuthal $E\times B$ electromagnetic flux [2]. If the trap configurations are kept axisymmetric, the particle number, electrostatic energy and canonical angular momentum within the NNP system are made highly conservational so that various paths of dynamics can proceed in practically loss-free isolated states. In this paper we overview various processes involved in instability, vortex dynamics, turbulence and formation of ordered structures that progressively appear starting from well-controlled initial conditions. The scope and framework of this paper is given in the next section. Main concern here is on the 2D dynamics including vortex (clearly observable distributions) and fine-scaled background distributions generating fluctuating electric fields that drive incoherent $E\times B$ flows. After these description, a short reference will be given on the contribution of Landau damping to the structure formation of 2D vortex column as an extra feature of plasmas in vortex dynamics.

2. Scope

Because this paper is written on the basis of experimental observations, fundamental procedures are described briefly (Sec. 3) Then the discussion proceeds as follows: first we discuss the formation process of ordered arrays of string distributions of electrons (often referred to as clumps) assisted by fluctuating background fields. Here we focus to the case where the clumps' distributions are quite narrow compared to the external structures driving the clumps so that the deformations of the clumps are not essential (Sec. 4). Discussion shall be extended to the cases where the background distribution is weakly unstable so that competitions occur in the growing patterns between the clumps' array and unstable modes (Sec. 5).

The discussion is extended further to the cases with many clumps immersed in different heights of background

author's e-mail: yash.kiwamoto@mbn.nifty.com

vorticity (density) distribution (BGVD) where the clumps repeatedly form ordered arrays with successively decreasing components under isolated relaxation (Sec. 6). Here in the transition to the next generation of ordered array, merging occurs among clumps. Therefore Sec. 7 is devoted to a brief description of basic processes in vortex merger, where internal deformations driven in the shear fields from other vortex are essential as well as the self-generated multipole fields. Coalescence of the core distributions is associated by the outward emissions of filamentary distributions so as to conserve the total energy and angular momentum. These topics suggest paths of structural evolution of the vortex or plasma flow systems depend sensitively on the initial configuration as well as incidental perturbations externally imposed.

The next topic, a core of this paper in Sec. 8 is the structural analyses of nonlinear stage of shear-flow driven diocotron (Kelvin-Helmholtz) instability. Here we extend the wave-number (k) space dynamics of energy and enstrophy ($\propto \zeta^2$) to include both scales ($\propto 1/k$) and spatial coordinates (x, y) by introducing multi-scale wavelet analyses. With this approach we shall see that eminently observable coherent vortices (blobs), generated in the initial nonlinear stage of the instability, successively decrease in number associated with the emission of filamentary distributions eventually absorbed into the turbulent background consistently with the energy spectrum $E(k) \propto k^{-3}$ as predicted for idealized stationary 2D turbulence. As the last topics, a brief comment will be given in Sec. 9 on the contribution of resonant particles in connecting the energy and momentum of high frequency waves to the 2D vortex dynamics.

3. Experimental Method

The vortex dynamics interacting with fluctuating background fields are studied with pure electron plasmas confined in traps consisting of a homogeneous magnetic field (B = 0.048 T or 1-2 T) and square-well potential. Various combinations of electron strings are injected in pulses through a lowered potential barrier and held in the trap until being relaxed to a desired shape of smooth distribution. If necessary, concave or hollow distributions are generated by slightly decreasing the barrier to push out the near-axis population by expulsive self-field. Desired arrays of electron clumps are then superposed onto the background population to complete the initial distribution [3].

After a pre-set time of holding, the potential barrier on the other side is removed to let the electrons escape along the magnetic field, accelerated by 5-7.5 kV and eventually collected on a Al-coated phosphor screen. The axially integrated electron distribution is recorded on a charge-coupled-device (CCD) camera as a 2D numerical array of luminosity that was experimentally confirmed to be proportional to the electron number. The absolute value of the total electron number is determined by time-integrating the measured current collected through the Aluminum film. The time history of the relaxation process is traced by repeating this destructive diagnostics after varied holding time. More detailed description may be found in Ref. [3].

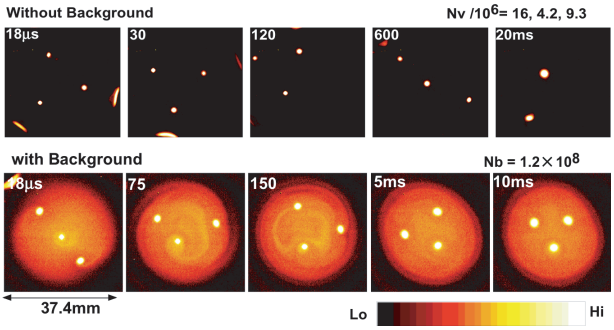

Fig. 1 Configurational relaxation of three point vortices with (lower) and without (upper) background distribution.

4. Formation of Ordered Array of Clumps

A string distribution of electrons parallel to magnetic field is referred to as a point vortex as long as the internal structures are not taken into consideration. Three point vortices initially placed at the vertices of an equilateral triangle are known both theoretically and experimentally to keep this configuration [4, 5]. However, as shown in the upper panels of Fig. 1, this initial configuration is not sustained in the presence of other perturbing forces than their mutual interaction such as contributions of image charges induced on a surrounding wall [6]. On the other hand, as shown in the lower panel, in the presence of the background population, linearly aligned point vortices form an equilateral array and keep this configuration for 0.5 s until atomic collisions take effects as dissipations [5].

Contributions in the formation and sustaining of the ordered arrays of the clumps are to be attributed to the fine structures and fluctuations, which are induced by the clumps, in the surrounding background distribution. The background's effect was quantitatively confirmed as the observation that the transient time required to reach the equilateral array from the linear array decreases as the electron number in the background increases [5].

5. Interaction of Clumps and Unstable Background

In cases that clumps are placed orderly in weakly unstable background distribution, structural evolutions were found to depend sensitively on relative strength of the two parts [7]. Some examples are shown in Fig. 2. In the absence of the clumps (1st panels), the initial distribution of the background in a hollow shape with a radial shear of azimuthal flow deforms spontaneously in $m = 2$ mode in a characteristic time of 200 μs.

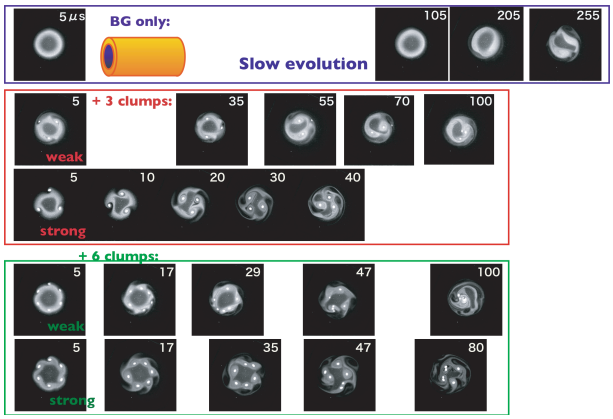

Fig. 2 Deformations in the clumps' configuration and weakly unstable background distribution in interaction.

The 2nd and 3rd panels show the cases where 3 clumps are superposed on the same background. While the electron number in the clumps is not large (2nd panel), the clumps are bunched into the $m = 2$ mode and accelerate the growth of the background's instability. On the other hand, if the clumps' densities are high, the BG is modulated in (originally stable) $m = 3$ mode or deforms into 3 blobs. Then $m = 2$ modulation (2 blobs) appears faster than the case of 1st panel. The same story is observed in the cases with 6 clumps as shown in the last two panels. These observations suggest that interactions among eminent elements and inconspicuous components tend to accelerate the appearance of either side of characteristics via mutual deformations.

6. Successive Decay and Re-Emergence of Vortex Crystals in Background Distribution

The process shown in Fig. 1 is examined further so as to include the merging of clumps and re-organization of ordered array with decreased number as shown in Fig. 3. The readers may notice the elongation of the time scale between each arrays of decreasing number of clumps. After the formation of the first crystal configuration, it is quite rare that unordered arrays are observed, but the number of the constituent clumps shows statistical dispersion after a given time of relaxation. This observation indicates that the turbulent period of clumps' dynamics, in which the clumps' merger proceeds, is much shorter than the life time of crystalized arrays.

The number of clumps in observed crystals is plotted in Fig. 4, starting from the same array of 14 clumps immersed in different levels of almost flat background distributions. The clumps' arrays in Fig. 3 are taken from the highest case of BGVD4. The horizontal arrows indicate the number of clumps composing the first crystal arrays. As the level of BGVD decreases, the appearance time of the first crystal delays and the number of clumps decreases.

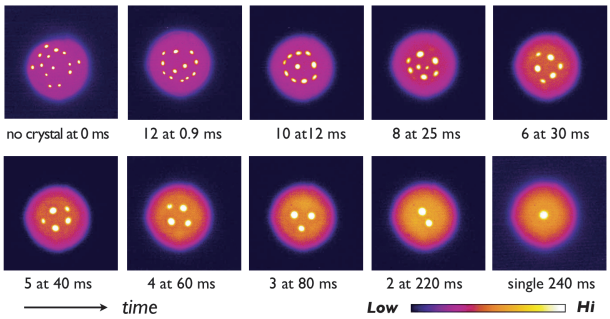

Fig. 3 Ordered arrays of clumps appearing during the relaxation from the initial distribution consisting of 14 clumps superposed on a BGVD4 with hight about 1/40 of the clumps [8].

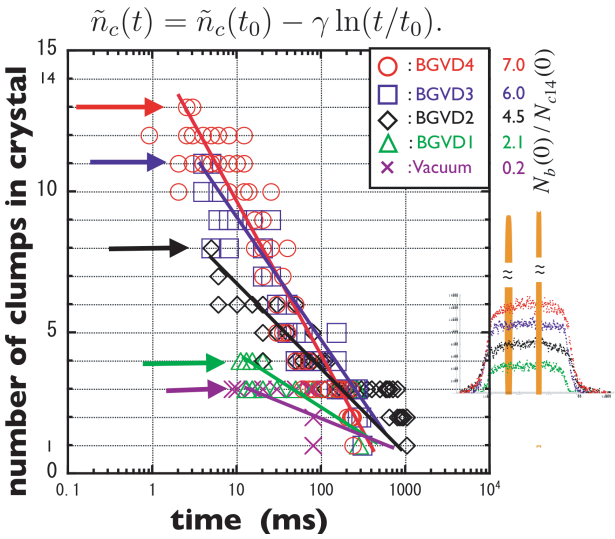

Fig. 4 The number of clumps forming crystal arrays plotted against the logarithm of time, starting from different levels of BGVD drawn on the right [8].

With the best control of the initial conditions, the observed processes remain stochastic in time.

The stochastic distributions of the observed data, however, are found to best fit to the log(t) vs. clumps number plot. In numerical simulations and laboratory experiments of free-decaying turbulence mainly composed of blobs with finite width, the number of blobs has been reported to obey the power law in time as $N_c \propto t^{-\xi}$ ($\xi = 1$) [9]. The data in the first report of vortex crystals in a pure electron plasma by Fine et al. [10] are also confirmed to show the logarithmic dependence in the crystal stage [8].

This new finding suggests that high and compact density (vorticity) distributions tend to establish highly ordered configurations under the influence of ambient fluctuating fields and, once formed, keep the configuration until some conditions are violated. The slope of fitting lines in Fig. 4, increasing with the BGVD height, suggests that fluctuations exerted by the BGVD tend to broaden the clumps width and make them vulnerable to the shear-

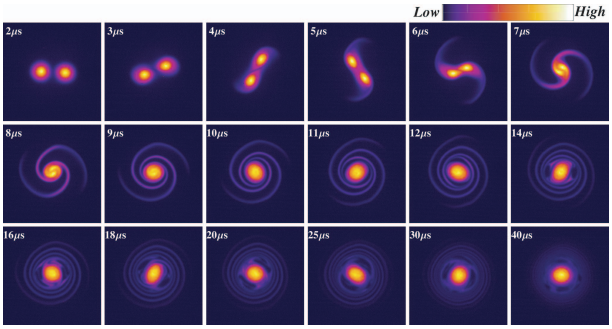

Fig. 5 Time evolution of electron density distributions under merging process [12].

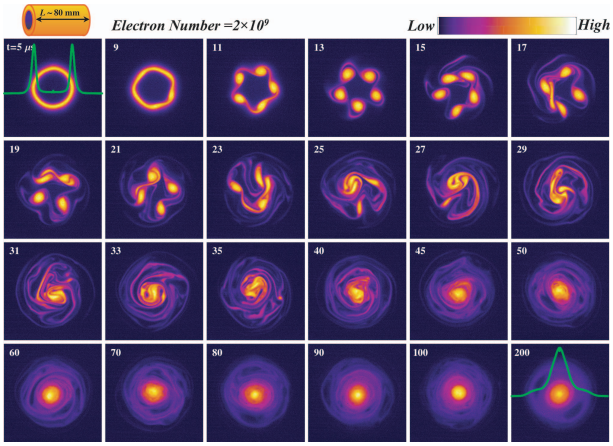

Fig. 6 Time evolution of electron density distribution starting from hollow profile with strong shear flow [13].

driven deformation that eventually leads to merger of the finite clumps. The time required for the deformation / merging and reorganization process will be observed to be much shorter than the life time of the quasi-equilibrium crystalized states in the following examinations.

7. Merger of Discrete Vortices

Broadening of the density distribution causes the merger of clumps. Figure 5 shows a structural evolution of merging identical vortices that are initially separated by 9.5 mm. The inter-vortex distance leading to merger lies around twice the diameter at half maximum [11], and our observations indicate that merger of two cores takes in about twice of the mutual rotation period. The merging process starts with deformation of the density distribution that is caused by the $E \times B$ shear generated by the counter part. The deformations generate an inward / outward $E \times B$ flow as well as the azimuthal flow inhomogeneously. The spiraling inward flow drives the merging of the two cores, while the filamentary distribution are driven outward. The two-way transports are essential to conserve the particle number (circulation), the energy and the canonical angular momentum of this isolated system throughout the re-distribution.

In the presence of a third distribution, the merger becomes available between far apart blobs. An addition of a low (even less than 1/10) density blob in between generates spiral filaments that cause deformations around the core of the two blobs and trigger the merger. This process may add another path to intermittent structural transitions of a macro system composed of multi-scales of distributions.

Incompressibility of two-dimensional guiding-center fluid is another interesting topic. Areas in the x-y plane occupied by different height of electron density are examined as a function of relaxation time over 512×512 pixels on the CCD image . The total number of pixels representing the presence of electrons is confirmed to remain constant. However, the areas belonging to the lower half of the density contours are observed to mix while the subtotal number is conserved. This re-distribution is eminent during the merger-dominated period where filamentary structures are produced and tightly wound, so that smoothing effect of viscosity needs to be taken into consideration. On the other hand, the areas occupied by the electrons belonging to the upper half of the density contours are observed to remain almost constant. This difference in the incompressibility is reflected in the longevity (coherent structure) of strong (high density) vortices and fluctuating unidentifiable small scale-eddies. Reasonable separation is one of the main topics in the next discussion on free-decaying 2D turbulence.

8. Free-Decaying 2D Turbulence Triggered by Shear-Driven Instability

In a hollow density distribution of electrons as schematically drawn at the top left of Fig. 6, strong radial shear is generated in the azimuthal $E \times B$ drift flow, and diocotron (Kelvin-Helmholtz) instability grows faster with increasing azimuthal mode numbers in the density distribution as the initial shell thickness decreases.

Within a few μs the deformation changes from linear growth into a nonlinear stage to generate corresponding number of strings. Because the strings are of finite width and the space in between is filled with low density population, merging processes set in concurrently as observed already in Fig. 5. Furthermore, since the average distribution is still of hollow shape with increased thickness, this system can be still linearly unstable to lower-mode instability as expected from Fig. 2. Driven by these destabilizing factors, the number of strings decreases successively in association with merger at the most vulnerable location until a single-peaked distribution forms in about 40 μs. During this merging process filamentary distributions are emitted radially and wound around the core part. The differential $E \times B$ rotations stretch and tighten the spiral distributions so as to generate further deformations into smaller scales that can further drive local transports.

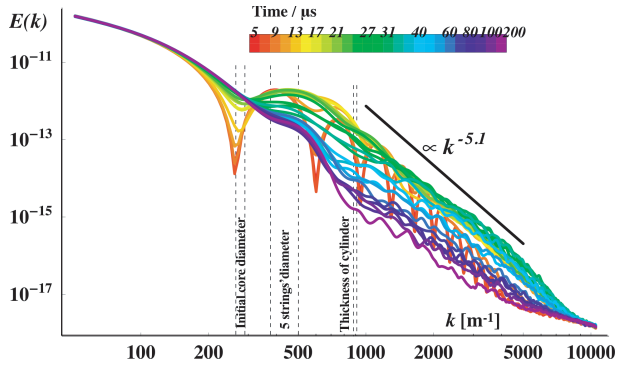

Fig. 7 Time evolution of the energy spectra in the vortex dynamics shown in Fig. 6 [13].

The Fourier analyzed energy spectra are evaluated as

$$E(k) = \frac{1}{2}\left(\frac{e}{\varepsilon_0 B_0}\right)^2 \int_0^{2\pi} k\mathrm{d}\varphi \frac{|n(\mathbf{k})|^2}{k^2}, \tag{1}$$

and plotted in Fig. 7 for each stage of the evolution displayed in Fig. 6. Dips in the red curve representing the initial distribution reflect the externally imposed clear-cut structure and associated harmonics.

The spectral dynamics are often presented in terms of transfer rates, $\varepsilon(k)$ and $\eta(k)$, of energy and enstrophy densities, $E(k)$ and $Z(k) = k^2 E(k)$ in the wave-number space defined as

$$\varepsilon(k) = -\int_{k_{\min}}^{k} \mathrm{d}k \frac{\partial E(k)}{\partial t}, \tag{2}$$

where $\eta(k)$ is defined in the same way. From the time-dependent spectra given in Fig. 7, the transfer rates are obtained as in Fig. 8. The positive value stands for upward transfer in the k space.

As theoretically expected in 2D turbulence, the energy cascades downward while the enstrophy exhibits upward cascade. The energy source in k space exists around k_{inj} corresponding to the distribution of 5 strings in Fig. 6 that grow within initial few μs. The downward cascade of energy corresponds to the merging process of the dominating finite strings toward a single peak, while the upward transfer of the enstrophy reflects the creation of spiral fine structures. The amplitudes of the transfer rates are measures of activity of the nonlinear mode couplings in the k space enhanced during the merger period among vortices in the (x, y) space. The clear correlation between $\varepsilon(k)$ and $\eta(k)$ suggests that the two-way cascades take place simultaneously.

This is consistent with theoretically predicted characteristics of 2D turbulence [9]. But we notice some discrepancies from the idealized model. The transfer rate $\varepsilon(k)$ is observed to peak around 0.6 k_{inj} and decreases at smaller k. This profile suggests that an endless downward flow of energy is blocked by the finite system size and in part by the absence of dissipation sufficient to compensate the energy input from above. This leads to the accumulation of

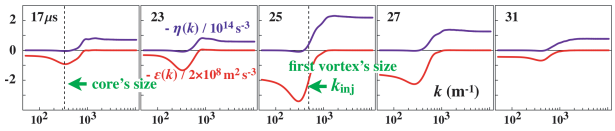

Fig. 8 Transfer rates of energy (red) and enstrophy (blue) in the wave-number space [13].

energy around k characterizing the single-peaked distribution as observed after 30 μs in Fig. 6. Though there should remain some freedom in reshaping the merged distribution, the NNP property of simultaneous conservation of electromagnetic canonical angular momentum may impose strong restriction in a large-scale transport.

The almost flat profile of $\eta(k)$ is consistent with the 2D turbulence model predicting that the source fluctuations around k_{inj} are transferred constantly up to dissipation scales. However observations in Fig. 7 indicate steeper power index of $\alpha = 4-6$ in the $E(k) \propto k^{-\alpha}$ fitting of the energy spectra. This steepness has been attributed to the presence of coherent vortices which remain distinguishable at low k while small-scale fluctuating eddies lose their identities. This feature may be discussed in terms of generation of characteristic structures interacting with ambient turbulence.

Examinations along this direction are explored by employing multi-scale resolution analysis with wavelets that provides scale-resolved structures as a function of coordinates [14]. Scale-resolved distributions $n(x, y, j)$ are derived for each density distribution already shown in Fig. 6, and plotted in Fig. 9 in squared form so as to be proportional to the local enstrophy. Here the scale base is proportional to 2^{-j}. The increase in $j = 5, 6$ components reflects the creation of filamentary structures during the mergers among strong vortices.

For discrimination of coherent components from the mixed total distribution we introduce a cumulative sum of squared wavelet coefficients, that generate the scale-resolved distributions in Fig. 9, in the order of amplitudes over all the scales as plotted in the middle of Fig. 10. Requiring lager coefficients to represent the coherent part, we examine the power index α in the energy spectra $E(k) \propto k^{-\alpha}$ of the coherent and incoherent (fluctuating) parts.

When the number of terms belonging to the coherent part is increased, there appears an abrupt transition in α from 8 to 5.5, while the power index of the incoherent part decreases continuously. Because there is no other reference for the discrimination discovered, we take the 34 terms sharing 88% of the total enstrophy as composing the coherent part. The energy spectra of thus separated components are plotted at the right of Fig. 10. The incoherent part is observed to be represented by $\alpha = 3$, which characterizes the idealized 2D turbulence in a stationary state.

The distributions reconstructed from the separated coefficients at 31 μs are shown in Fig. 11 exhibiting highly

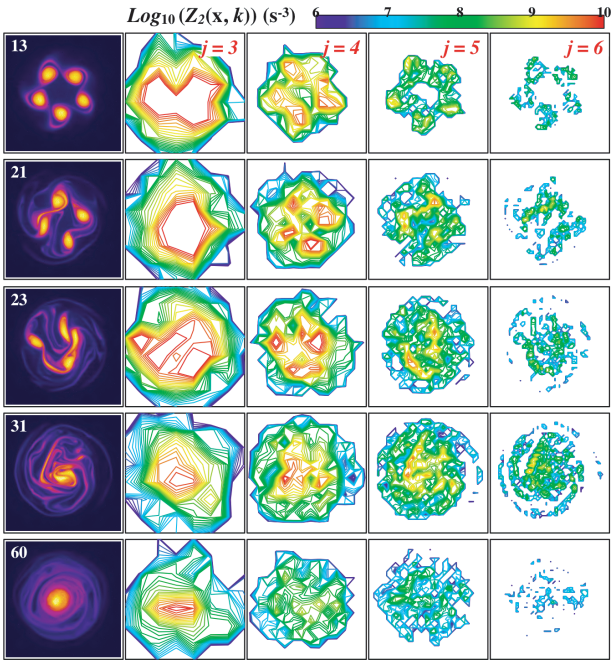

Fig. 9 Time and scale resolved enstrophy distribution [14].

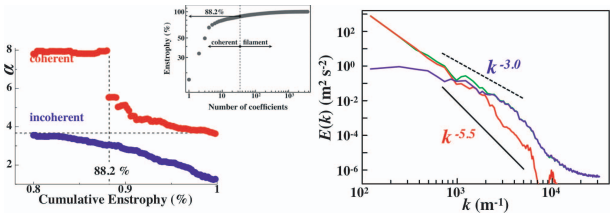

Fig. 10 Procedure of separating coherent and fluctuating parts in vortex dynamics to determine each energy spectrum [14].

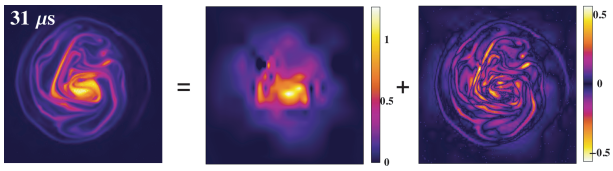

Fig. 11 Spatial distribution at 31 μs separated into coherent and incoherent parts [14].

filamentary structures within the incoherent or "turbulent" part on the right. Note the fluctuating distribution consists of both positive and negative parts.

9. NNP Properties beyond 2D Euler Fluid

That NNPs consist of single-signed particles adds another properties beyond the neutral Euler fluid. One is the canonical angular momentum that is dominated by electromagnetic contribution associated with Poynting vector ($\propto E \times B$) over the mass-dependent kinetic momentum by several orders of magnitude. The second is a characteristic property of plasmas, the microscopic interaction of resonant particles with collectively oscillating electric fields, i.e. Landau damping. High-frequency (HF) oscillations have been observed to be excited simultaneously with generation of a hollow initial distribution as in Fig. 6 and persists for a long period of vortex relaxation in an axisymmetric mode without observable effects on the vortices [15]. These oscillations have been identified to be $m = 0$ dominant Trivelpiece-Gould mode extending over multiple vortex columns.

However, when HF electric fields are applied externally with non-zero azimuthal mode number ($m \neq 0$) onto multiple columns of electrons, as far as we have observed, the electrons are driven out irregularly to the surrounding wall. Orderly compression and expansion of the density profile have been observed exceptionally, only when the density distribution is prepared axi-symmetric and HF fields have non-zero azimuthal mode number. This has been known empirically for a while as rotating wall technique to prevent radial losses due to dissipations or inevitable irregularities in confining configurations or to compress NNP to higher density for anti-matter experiments [16].

Theoretical and experimental examinations have revealed that essence of the NNP and HF-fields interaction lies in the axial Landau-damping of the resonant particles that accompanies net radial transport driven by oscillating $E \times B$ drifts of resonant particles. The canonical angular momentum of the NNP is varied through the torque resonantly applied from the rotating azimuthal HF electric field. Theoretical analyses predict that the Landau-damped HF field energy is 100% converted to the axial kinetic energy and the potential energy with a partition rate of $(\omega - m\omega_E) : m\omega_E$, where $\omega_E(r)$ is the azimuthal rotation frequency of zero-th order [17]. This prediction has been confirmed experimentally [18]. These examinations suggest that Landau-damping may be playing significant roles behind observable dynamics of macroscopic structures.

10. Conclusion

Physical processes toward generation of ordered structures are discussed by taking the vortex and turbulent dynamics of strongly magnetized pure electron plasmas as a test bed. High density elements (clumps) are observed to be driven by low-density background populations toward the formation of ordered structures, for which fluctuating fields generated in the mutual interactions of both parts are observed to be essential as well as for destroying it to establish the next generation of ordered structure. The dynamic system is also found to be separated into coherent components and turbulent parts of short life bearing characteristic energy spectrum of 2D turbulence. It is also pointed out that macroscopic structures within highly conservational systems can be externally controlled via Landau damping of high-frequency electric fields.

The authors appreciate stimulating discussions with Prof. K. Itoh at NIFS and with Prof. M.Y. Tanaka in Kyushu Univ.in the course of this research, which has been continuously supported by the Grant-in-Aid of JSPS since 1999 to 2009 and partly by the collaborative program of NIFS since 2001 to 2007.

[1] C.F. Driscoll and K.S. Fine, Phys. Fluids B **2**, 1359 (1990).
[2] T.M. O'Neil, Phys. Fluids **23**, 2216 (1980).
[3] Y. Kiwamoto *et al.*, Phys. Rev. Lett. **85**, 3173 (2000).
[4] H. Aref, Phys. Fluids **22**, 393 (1979).
[5] A. Sanpei *et al.*, Phys. Rev. E **68**, 016404 (2003).
[6] I.M. Lansky and T.M. O'Neil, Phys. Rev. E **55**, 7010 (1997).
[7] D. Fujita *et al.*, Plasma and Fusion Res **1**, 144 (2006).
[8] Y. Kiwamoto *et al.*, Phys. Rev. Lett. **99**, 115002 (2007).
[9] U. Frish, *Turbulence* (Cambridge Univ. Press, 1995).
[10] K.S. Fine *et al.*, Phys. Rev. Lett. **75**, 3277 (1995).
[11] C.F. Driscol and K.S. Fine, Phys. Fluids B **2**, 1359 (1990).
[12] Y. Suzuki (from Graduation thesis, Kyoto Univ. 2007)
[13] Y. Kawai *et al.*, Phys. Rev. E **75**, 066404 (2007).
[14] Y. Kawai and Y. Kiwamoto, Phys. Rev. E **78**, 036401 (2008).
[15] Y. Kawai *et al.*, Phys. Plasmas **14**, 102106 (2007).
[16] F.A. Anderegg *et al.*, Phys. Rev. Lett. **81**, 4875 (1998).
[17] Y. Kiwamoto *et al.*, Phys. Plasmas **12**, 094501 (2005).
[18] Y. Soga *et al.*, Phys. Plasmas **13**, 052105 (2006).